



Originally published as:

Koch-Müller, M., Mugnaioli, E., Rhede, D., Speziale, S., Kolb, U., Wirth, R. (2014): Synthesis of quenchable high-pressure form of magnetite (h-Fe₃O₄) with composition Fe₁(Fe₂+0.75Mg_{0.26})Fe₂(Fe₃+0.70Cr_{0.15}Al_{0.11}Si_{0.04})₂O₄. - *American Mineralogist*, 99, 11-12, pp. 2405—2415.

DOI: <http://doi.org/10.2138/am-2014-4944>

Synthesis of quenchable high-pressure form of magnetite (h-Fe₃O₄) with composition $\text{Fe}^{\text{I}}(\text{Fe}^{2+}_{0.75}\text{Mg}_{0.26})\text{Fe}^{\text{II}}(\text{Fe}^{3+}_{0.70}\text{Cr}_{0.15}\text{Al}_{0.11}\text{Si}_{0.04})_2\text{O}_4$

Monika Koch-Müller¹, Enrico Mugnaioli^{2,3}, Dieter Rhede⁴, Sergio Speziale¹, Ute Kolb^{2,5}, Richard Wirth¹

¹ Sektion 3.3, Chemie und Physik der Geomaterialien, Deutsches GeoForschungsZentrum, Telegrafenberg, 14473 Potsdam, Germany

² Institut für Physikalische Chemie, Johannes Gutenberg-Universität, Jakob-Welder-Weg 11, 55128 Mainz, Germany

³ University of Siena, Department of Physical sciences, Earth and Environment, Via Laterina 8, 53100 Siena, Italy

⁴ Sektion 4.2, Anorganische und Isotopenchemie, Deutsches GeoForschungsZentrum, Telegrafenberg, 14473 Potsdam, Germany

⁵ Institute für Angewandte Geowissenschaften, Technische Universität Darmstadt, Schnittspahnstr. 9, 64287 Darmstadt, Germany.

keywords: Fe-oxide, h-Fe₃O₄, high-pressure, electron transmission microscopy, electron diffraction tomography, electron energy loss spectroscopy, electron microprobe analyses, crystal chemistry

Abstract

We report the synthesis of h-magnetite, ideally h-Fe₃O₄ with considerable amounts of substitutional cations (Cr, Mg, Al, Si) and quenchable to ambient conditions. Two types of experiments were performed at 18 GPa and 1800 °C in a multi-anvil press. In one, we used an oxide mixture with a majoritic stoichiometry Mg_{1.8}Fe_{1.2}(Al_{1.4} Cr_{0.2}Si_{0.2}Mg_{0.2})Si₃O₁₂, with Si and Mg in excess as starting material (MA-367, MA-380). In the second type of experiment (MA-376), we started from an oxide mixture on the composition of the Fe-oxide phase obtained in MA-367. The Fe-oxide phases of both experiments were investigated by electron microprobe and transmission electron microscopy including electron diffraction tomography. Our investigations show that the Fe-oxide phases crystallize in the structure-type of h-magnetite. However, electron diffraction data show that keeping the cell setting from literature, this phase crystallizes in space group *Amam* and not in space group *Bbmm* as previously proposed. In the experiment MA-367, the Fe-oxide phase are mutually intergrown with majorite, the major phase of the run products. The formula for h-magnetite in this run was calculated as $^{\text{Fe1}}(\text{Fe}^{2+}_{0.75} \text{Mg}_{0.26})^{\text{Fe2}}(\text{Fe}^{3+}_{0.70} \text{Cr}_{0.15}\text{Al}_{0.11} \text{Si}_{0.04})_2\text{O}_4$. In the experiment on the bulk composition of the Fe-oxide, the main phase was h-magnetite with composition $^{\text{Fe1}}(\text{Fe}^{2+}_{1.02})^{\text{Fe2}}(\text{Fe}^{3+}_{0.65} \text{Cr}_{0.19}\text{Al}_{0.13} \text{Si}_{0.03})_2\text{O}_4$ and traces of nearly pure end-member wadsleyite and stishovite. Our results indicate that the substitution of 20 to 30% of Fe (0.7 to 0.9 atoms per formula unit) by smaller cations favored the preservation of the high-pressure form to ambient conditions. We prove that the h-magnetite-type oxide is also stable in chemical systems more complex than Fe-O. Based on our results, which were obtained at 18 GPa and 1800 °C in a system (MA-367) that is closely related to Fe-enriched oceanic lithospheric material, we suggest that a Fe₃O₄-rich phase may be present in environments connected to deeply subducted slabs and possibly associated with deep carbonatitic melting. Our observations show that Cr strongly partitions in the oxide phase such that the coexisting

silicates are depleted in Cr compared to Fe₃O₄-free assemblages. This may significantly affect the chemical signature of melts produced in the deep mantle.

Introduction

The discovery of the high-pressure Fe-oxide Fe₄O₅ (Lavina et al. 2011) revealed that the Fe-oxide phase relations, especially at high pressures, are still poorly understood. Under ambient conditions, the Fe-oxides FeO (wüstite), Fe₃O₄ (magnetite) and Fe₂O₃ (hematite) are stable and form complex defect structures. Stoichiometric FeO is very difficult to synthesize – wüstite chemical composition is more realistically written as Fe_{1-x}O (Hazen and Jeanloz 1984). It crystallizes in the cubic NaCl-type structure and forms a solid solution series with MgO (periclase). Magnetite is a cubic inverse-spinel-type ferrite whose unit cell contains eight Fe³⁺ in the tetrahedral sites, and a “uniform”, mixed-valence occupancy of 8 Fe²⁺ + 8 Fe³⁺ in the octahedral sites. Common impurities in natural magnetite are traces of Mg, Zn, Mn, Ni, Cr, Ti, V (Bowles et al. 2011). Fe₂O₃ occurs in different modifications, with hematite (α-Fe₂O₃) as the most prominent one. Hematite is known to incorporate traces of Ti, Al, and Mn (Bowles et al. 2011).

All three Fe-oxides show non-quenchable, pressure-induced phase transitions. According to Ono et al. (2004) hematite transforms at 30 GPa and 1800–2200° C into a perovskite-type structure. Wüstite at ambient temperature transforms at pressure above 17 GPa into a rhombohedral or monoclinic polymorph (Zou et al. 1980; Shu et al. 1998; Fei 1996; Kantor et al. 2008; Fisher et al. 2011) and to a NiAs-type polymorph at pressures above 60 GPa and high temperatures (e.g. Fei and Mao 1994; Kondo et al. 2004).

The phase diagram of Fe₃O₄ is still controversial. According to Pasternak et al. (1994), cubic inverse-spinel magnetite transforms at $P > 25$ GPa and room temperature to a monoclinic high-pressure phase. Dubrovinsky et al. (2003) and Lazor et al. (2007) propose $P > 19$ GPa as

pressure for the transition of magnetite to h-magnetite at room temperature. In a Mössbauer and X-ray diffraction study, Rozenberg et al. (2007) reported a pressure-induced transformation of inverse magnetite to normal-spinel magnetite at 8 GPa. However, Glazyrin et al. (2012) did not observe for magnetite the inverse to normal spinel transition nor the transformation to h-Fe₃O₄ at pressures up to 21 GPa. On the other side Bengtson et al. (2013) predict in a theoretical ab initio study a phase transition from inverse-spinel magnetite to h-Fe₃O₄ at 10 GPa. According to them there is no inverse- to normal-spinel transition in magnetite.

The symmetry of h-magnetite, initially interpreted as monoclinic (Pasternak et al. 1994) has also been subject of controversy. In a synchrotron X-ray diffraction study, Fei et al. (1999) found that h-Fe₃O₄ is not monoclinic but isotypic with CaMn₂O₄ (space group *Pbcm*), with all Fe³⁺ ions in octahedral sites and Fe²⁺ in eightfold-coordinated sites, which are described as bicapped trigonal prisms. Haavik et al. (2000) pointed out that their X-ray data were also consistent with the CaTi₂O₄ structure-type (space group *Bbmm*). Space group *Bbmm* for the h-Fe₃O₄ structure has been confirmed by Lazor et al. (2004), Dubrovinsky et al. (2003) and Bengtson et al. (2013). Dubrovinsky et al. (2003) suggest that Fe²⁺ occupies trigonal prism (Fe1) with an average Fe1-O distance of 2.058 Å and that Fe³⁺ occupies octahedra (Fe2) with average Fe2-O distance of 1.961 Å.

The high-pressure Fe-oxide, Fe₄O₅ is stable from 5 to at least 30 GPa, and is recoverable to ambient conditions (Lavina et al. 2011). They synthesized Fe₄O₅ in a pure Fe-O system, using mixtures of Fe and Fe₃O₄ as starting material, at *P* = 10 and 20 GPa, and *T* between 1227 and 1927 °C and refined the structure as isostructural with CaFe₃O₅ (space group *Cmcm*). In the proposed structure, the atomic arrangement consists of two non-equivalent, edge-sharing FeO₆ octahedra (Fe1 and Fe2), which form layers perpendicular to the *c*-axis, alternating with layers of face-sharing trigonal prisms (Fe3). Thus, the structure is very similar to h-Fe₃O₄. Lavina et al. (2011) speculate that synthetic Fe₄O₅ may show stacking disorder involving

Fe₄O₅ and h-Fe₃O₄ octahedral layers may occur. In an in situ high-pressure X-ray diffraction study, Woodland et al. (2012) observed that cubic magnetite breaks down to a mixture of hematite and Fe₄O₅ between 9.5 to 11 GPa and 700 to 1400 °C, in disagreement with Schollenbruch et al. (2011) who observe an isochemical transition to h-magnetite in the same pressure and temperature regime. Woodland et al. (2012) suggested that the two coexisting phases, hematite and Fe₄O₅, recombine at higher pressures to form h-Fe₃O₄. Woodland et al. (2013) investigated the stability of Fe₄O₅ in several simple chemical systems and they found, e.g., that Fe in the Fe₄O₅ phase can be substituted by considerable amounts of other cations, e.g., Cr³⁺.

Until now, h-Fe₃O₄ has been investigated only as a pure Fe-oxide and it has never been recovered at ambient conditions. There is no information about Fe³⁺/ΣFe_{tot} ratio and possible incorporation of cations other than iron. Here, we report crystal chemical and structural data of this high-pressure Fe-oxide synthesized at 18 GPa and 1800 °C using: (1) an oxide mixture with a SiO₂ concentration close to that of the bulk silicate Earth (O'Neill and Palme 1998) and (2) a Fe-dominated oxide mixture plus Cr-, Mg- and Si-oxides. Surprisingly, the structure was quenchable in both types of experiments to ambient conditions, which allowed us to collect precise electron diffraction data by automated electron diffraction tomography (ADT). With this technique, we were able to deliver crystallographic information for single nanocrystalline domains in a polyphasic mixture. We observe that h-magnetite coexisting with the silicates is strongly enriched in Cr, and we speculate on the effects that such partitioning might impose on the concentration of Cr in the coexisting silicates and in melts produced in the deep mantle.

Experimental methods

A. Synthesis

We performed three multi-anvil runs with a 10/5 assembly, rhenium heater, and type C thermocouples at $P = 18$ GPa and $T = 1800$ °C for 6 hours. Two experiments, MA-367 and

MA-380, used a homogenous oxide mixture with 44.6 wt% SiO₂, 19.3 wt% MgO (annealed at 1200 °C), 15.7 wt% FeO, 17.1 wt% Al₂O₃, and 3.3wt % Cr₂O₃ placed in Fe-doped Pt-capsules (about 3 wt% Fe) to reduce the potential loss of Fe (e.g., Grove 1981). In these two runs we produced assemblages with majorite as the major phase and three additional minor phases: stishovite, magnesite, and a Fe-oxide with the composition given in Table 1. We intentionally did not remove traces of adsorbed water or CO₂ in the starting materials as this may have served as a flux to enhance the growth of large crystals. The presence of CO₂ and water explains the formation of traces of magnesite in the run products and goethite as alteration product during quenching (see below). To achieve large crystals in the second run (MA-380), the temperature of 1800 °C was cycled by 20 °C for the first 30 min of the run duration. The starting material of the third run was a homogenous oxide mixture with 42 wt% FeO, 34 wt% Fe₂O₃, 13 wt% Cr₂O₃, 6 wt% Al₂O₃, and 5 wt% SiO₂ also placed in Fe-doped Pt-capsules to reduce the potential loss of Fe. At the end of all runs temperature was quenched to ambient conditions within 2 minutes, and the decompression time was 43 h to avoid breakage of the WC cubes. The 10/5 assembly was calibrated using the following phase transitions: coesite–stishovite (Akaogi et al. 1995), α–β Mg₂SiO₄ (Morishima et al. 1994), β–γ Mg₂SiO₄ (Inoue et al. 2006), enstatite–β Mg₂SiO₄–stishovite (Gasparik 1989). All the syntheses were performed at the high-pressure laboratory of the German Research Centre for Geosciences (GFZ) in Potsdam.

B. Electron microprobe analyses

Multi-phase aggregates of products from all three experiments were embedded in epoxy and polished for the electron microprobe (EMP) measurements. The chemical composition of the phases was determined by wavelength-dispersive X-ray analysis (WDS) techniques using a JEOL JXA-8500F (HYPERPROBE) electron microprobe at the GFZ in Potsdam. The analytical conditions included an acceleration voltage of 15 kV, a beam current of 20 nA, and a beam diameter of 1 μm. The following natural and synthetic standards were used (with the

respective element and peak counting time listed in parentheses): diopside (for Mg; 40 s, Si; 40 s, Ca; 40 s), hematite (for Fe; 40 s) and Cr₂O₃ (for Cr; 40 s). The background counting times were always set to half of the respective peak counting times. The CITZAF routine in the JEOL software was used for data processing. Element distribution maps were produced in WDS mode using an accelerating voltage of 15 kV and a beam current of 20 nA. We accumulated a 500 × 400 pixel frame with a step size of 0.5 μm and a dwell time of 200 ms per pixel in stage-scanning mode. We could not obtain satisfactory analyses of magnesite, which was instead identified by Raman spectroscopy (Supplemental Fig. 1¹), because it was not stable under the electron beam.

C. X-ray diffraction

X-ray diffraction patterns of compact multi-phase aggregates of the run products MA-367 and MA-376 about 100 μm in size were collected using a Rigaku R/AXIS200 SPIDER diffractometer operating at 40 kV and 30 mA at GFZ. The samples were mounted on CryoLoops (Hampton Research), and the loops were placed into a goniometer. During data acquisition the goniometer holding the sample was rotated continuously at a speed of 2 ° per s over 360°. A rotating Cu anode served as the X-ray photon source. The detection system consists of a cylindrically shaped image plate, which reads out the diffracted radiation in a 2θ range of – 60 to 144° in horizontal and +/- 45° in vertical direction. LeBail refinement was done using the GSAS software package (Larson and Van Dreele 1998). Starting values for the refinements were the fractional atomic coordinates and lattice parameters for majorite, stishovite, and magnesite taken from the ICSD database (Belsky et al. 2002), the inorganic structure database. For h-Fe₃O₄ we used the results obtained from our automated electron diffraction tomography analyses (ADT).

Powder XRD patterns for MA-376 were also recorded in transmission using a STOE STADI P diffractometer (CuKα₁ radiation), equipped with a primary monochromator and a 7° wide

¹ Deposit item AM-14-1110, Supplemental Table, Figure and CIF. Deposit items are stored on the MSA web site and available via the *American Mineralogist* Table of Contents. Find the article in the table of contents at GSW (ammin.geoscienceworld.org) or MSA (www.minsocam.org), and then click on the deposit link.

position sensitive detector at the GFZ Potsdam. A part of the run product was ground to a final grain size of about 5 μm , diluted with Elmer's white glue and spread on a circular amorphous foil. The foil was placed into a transmission sample holder and covered with a second foil. Intensities were recorded in the range of 2Θ from 9° to 125° with a detector step size of 0.1° and a resolution of 0.02° . A 1 mm thick Al-foil was placed in front of the detector to reduce fluorescence radiation in the Fe-rich sample. Counting time was selected to yield a maximum intensity of 5000 counts. Unit cell were refined using the GSAS software package for LeBail refinements (Larson and Von Dreele 1987). Starting values for the refinements were the fractional atomic coordinates and lattice constants for h- Fe_3O_4 from our ADT analyses.

D. Transmission electron microscopy

Electron-transparent foils of sample MA-367 and MA-376 for transmission electron microscopy (TEM) were prepared at the TEM Laboratory of the GFZ by a focused ion beam (FIB) milling technique (Wirth 2009). Foils with the dimensions $15 \times 10 \times 0.150 \mu\text{m}^3$ were cut with a FEI FIB200TEM device using Ga-ions accelerated to 30 keV from the polished section of the sample on spots which were identified as Fe-oxide.

Automated electron diffraction tomography (ADT) was carried out with a FEI TECNAI F30 ST transmission electron microscope operating at 300 kV at the Johannes Gutenberg-Universität in Mainz. ADT has already been used for the structure characterization of high-pressure experimental products, like the hydrous Al-bearing pyroxene HAPY (Gemmi et al. 2011). We investigated both, FIB foils from MA-367 and MA-376 and micrometric grains (μ -crystals) selected with a micromanipulator. Samples were deposited on carbon-coated copper grids. In total nine ADT data sets were collected from MA-367 (four sets from μ -crystals and five sets from different areas of the FIB foil) and eight ADT data sets were collected from sample MA-376 (three sets from μ -crystals and five sets from different areas of the same FIB foil).

ADT was carried out using the automatic module described in Kolb et al. (2007). Each ADT data collection was performed in tilt steps of 1° , for total tilt ranges of $90\text{-}120^\circ$. Electron diffraction patterns were acquired in nano-beam electron diffraction (NED) mode, with a quasi-parallel illumination obtained using a condenser aperture (C2) of $10\ \mu\text{m}$. The beam on the sample had a diameter of $70\ \text{nm}$. Crystal position was tracked after each tilt step in μ -probe scanning transmission electron microscopy (μ -STEM) mode. Data sets were collected both with and without precession of the beam [precession electron diffraction, PED, for details see Vincent and Midgley (1994); Mugnaioli et al. (2009)]. Data sets without precession were used for accurate cell parameter determination, while data sets with precession were used for reflection intensity extraction.

ADT data were analyzed using the ADT3D software (Kolb et al. 2008, 2011; Mugnaioli et al. 2009; Kolb et al. 2011; Schlitt et al. 2012), including three-dimensional diffraction reconstruction and visualization, cell determination, and reflection intensity integration. Ab initio structure solution was performed by direct methods using SIR2011 (Burla et al. 2012). Conventional in-zone electron diffraction patterns were recorded on the FIB-foils in a Tecnai F20-X-Twin microscope with a field emission gun as the electron source at the TEM Laboratory of the GFZ in Potsdam. The TEM is equipped with a Gatan imaging filter (GIF Tridiem), a Fishione high-angle annular dark field detector (HAADF), and an EDAX X-Ray analyzer. Energy-dispersive spectra were collected for 30 s on different spots of the sample to identify the phase of interest and to ensure that the additional elements are intrinsic to the Fe-oxide. Electron diffraction patterns were recorded from these sites with image plates. Fe^{3+} concentration was determined with electron energy-loss spectroscopy (EELS), applying the technique described by van Aken and Liebscher (2002). Spectra were acquired in the diffraction mode with a camera length of $700\ \text{mm}$. Convergence angle was $2\ \text{mrad}$, and the collection angle at the camera length used was $10\ \text{mrad}$ with a GIF entrance aperture of $2\ \text{mm}$.

Dispersion was 0.1 eV/channel. The energy resolution of the filter was 0.9 eV at full-width at half maximum of the zero loss peak.

E. FTIR spectroscopy

To check for the presence of intrinsic OH, IR spectra were taken at the FTIR Laboratory to the GFZ on single crystals of majorite and multiphase aggregates containing the Fe-oxide from run MA-380. Spectra were recorded on a Bruker Vertex 80v FTIR spectrometer, equipped with a Globar light source, a KBr beam-splitter and a Hyperion microscope using Cassegrainian objective and an InSb detector. Spectra were taken with aperture sizes depending on the crystal and aggregate size from 50×50 to $50 \times 100 \mu\text{m}^2$ and a resolution of 2 cm^{-1} . Spectra were averaged over 256 scans.

Results

Optical analyses of the products of MA-367 in transmitted light revealed that the major phase is a yellowish, isometric phase up to $30 \mu\text{m}$ in diameter, identified later as majorite, accompanied by an opaque phase, often appearing as elongated aggregates with 10 to $30 \mu\text{m}$ long and later identified as h- Fe_3O_4 . In addition, we identified two additional colorless phases, stishovite and magnesite, of the same small size. The same phases were also identified in the second run MA-380. In the latter, the majorite crystals were on average much larger than in sample MA-367, (up to $100 \mu\text{m}$). Obviously, *T*-cycling of the run produced larger single crystals of the garnet phase. Optical examination of the products of MA-376 in transmitted light revealed that it is completely opaque powder.

Electron microprobe analyses

Electron microprobe analyses confirmed that the product of run MA-367 consist of four phases: majorite [$\text{Mg}_{1.98}\text{Fe}_{1.05}(\text{Al}_{1.61}\text{Cr}_{0.11}\text{Si}_{0.11}\text{Mg}_{0.16})\text{Si}_3\text{O}_{12}$], nearly pure stishovite ($\text{Si}_{0.98}\text{Al}_{0.02}\text{O}_2$), a carbonate with composition of $(\text{Mg}_{0.8}\text{Fe}_{0.2})\text{CO}_3$, and a Cr-, Mg-, Al-, and Si-containing Fe-oxide (Figs. 1a and 1c; Table 1). According to the results of the TEM analysis the normalization procedure for the Fe-oxide was performed on the base of four O atoms and

to account for the presence of Fe^{3+} , we assumed the stoichiometry $\Sigma\text{M}/\text{O} = 0.75$. The calculated formula for the Fe-oxide is $(\text{Fe}^{3+}_{1.39}\text{Fe}^{2+}_{0.75}\text{Cr}_{0.29}\text{Mg}_{0.26}\text{Al}_{0.21}\text{Si}_{0.08})_{\Sigma=3}\text{O}_4$. The microprobe analyses of magnesite showed a relatively constant composition of about $\text{Mg}_{0.8}\text{Fe}_{0.2}\text{CO}_3$ (based on six analyses). The presence of ferroan magnesite as an impurity has been confirmed by Raman spectroscopy (the Raman peaks are shifted to lower wavenumbers compared to the pure magnesite end-member, thus confirming Fe-Mg substitution; Supplemental Fig. 1¹).

Electron microprobe analyses further revealed that the run products of MA-380 consist of Mg-rich majorite, nearly pure stishovite ($\text{Si}_{0.98}\text{Al}_{0.02}\text{O}_2$), and a Cr-, Mg-, Al- and Si-containing Fe-oxide (Fig. 1b). The crystal size of the Fe-oxide phase in the polished section of run MA-380 was too small to obtain sufficiently good chemical analyses, and the oxide sums are always approximately around 90%.

Electron microprobe analyses revealed that the product of run MA-376 consists of three phases: the major phase is a Cr-, Al-, Si-, and Mg-containing Fe-oxide and in addition traces of stishovite and nearly pure Mg-end-member wadsleyite (Fig. 1d). The composition of the Fe-oxide phase present in MA-376 is slightly different with respect to that in MA-367 as it does not incorporate magnesium and is thus more Fe-rich. The calculated formula for the Fe-oxide normalized to four oxygen is $(\text{Fe}^{3+}_{1.30}\text{Fe}^{2+}_{1.02}\text{Cr}_{0.37}\text{Al}_{0.25}\text{Si}_{0.05})_{\Sigma=3}\text{O}_4$.

X-ray diffraction and Transmission electron microscopy analyses

MA-367. We collected X-ray diffraction patterns on several aggregates of MA-367 using the Rigaku diffractometer and could identify majorite as the major phase plus stishovite plus magnesite. Some patterns showed weak reflections at about $2\Theta_{\text{Cu}} 33.2^\circ$, 33.8° , and $37.5 - 37.6^\circ$ (listed by decreasing intensity) that could not be explained either with the phases mentioned above or with other known oxide phases. Therefore the Fe-oxide phase of the sample was further investigated using automated electron diffraction tomography. ADT data revealed that the sample MA-367 contains two different Fe-oxide phases, which we call α -

phase and β -phase for simplicity. The α -phase is always predominant compared to the β -phase. Data acquired from μ -crystals show that the two phases usually appear together and that the diffraction images contain strong signals of the α -phase in addition to weaker signals from the β -phase. However, in the FIB foils it was possible to recognize areas where the two phases are clearly separated and in these areas it was possible to acquire ADT data from each of them. Figure 2 shows a high-angle annular dark-field image (HAADF) image (camera length 330 mm) of a FIB foil cut from a Fe-oxide grain of this sample. Fe-oxide grains consist of coherent areas of α -phase, separated by planar deformation features filled with the β -phase.

ADT structure analysis of the α -phase: Detailed analyses of the ADT data sets of sample MA-367 revealed that the α -phase crystallizes in the h-magnetite structure [Haavick et al. (2000) in situ X-ray powder diffraction (XRPD) at $P > 22$ GPa]. This was a surprise because h-magnetite is known to be unquenchable to ambient condition. All ADT data sets taken on the α -phase were consistent with an orthorhombic cell with parameters $a = 9.8(2)$, $b = 9.6(2)$, $c = 2.87(6)$ Å (Figs. 3a and 3b). These values are close to the cell parameters determined for h -Fe₃O₄ by Haavick et al. (2000) on the basis of XRPD. The analysis of the three dimensional reconstructed diffraction volumes revealed always the presence of two main extinction rules: $hkl : k + l = 2n$ and $h0l : h = 2n$, consistent with space groups $Amam$, $Ama2$, and $A2_1am$ (Table 2). These extinction rules are not consistent with Haavick's space group $Bbmm$. $Amam$ and $Bbmm$ are both not conventional settings of space group $Cmcm$ (63), but represent physically different objects when the cell parameter setting is fixed (in our case a = 'long', b = 'medium', c = 'short'). The difference between our ADT and Haavick's findings can be reconciled exchanging the a and b parameter. There are two possible explanation for this difference: (1) there is a real structural modification related with the introduction of Mg and Cr and/or the quenching of the material, and (2) there is an error in the determination of cell parameters or extinctions either by ADT or XRPD data. We point out that, despite the high error (2%) related with a single ADT cell determination (Kolb et al. 2011), the evidence that a is always

longer than b and that the presence of extinctions consistent with space group $Amam$ were always confirmed by all the independent ADT acquisitions. On the other hand, in presence of close a and b cell parameters and low quality XRPD data [as the ones available by Haavick et al. (2000)], it is not trivial to discriminate between space groups $Amam$ and $Bbmm$. For a matter of clarity, we report in Table 2 the extinction rules associated with these two space groups. Swapping a and b axes, the two space groups can be exchanged. According with the orthorhombic setting, reflection intensities were integrated for the two best ADT acquisition series, both performed with beam precession (Mugnaioli et al. 2009). Experimental details are given in Table 3. Ab initio structure solution was performed independently for the two data sets by direct methods implemented in SIR2011 (Burla et al. 2012), using scattering factors for electrons (Doyle and Turner 1968) and kinematic approximation (I_{hkl} proportional to F_{hkl}^2). Structure solution converged in space group $Amam$. Only the solution automatically picked by the SIR2011, i.e., the one with the lowest residual, was considered. The resulting potential maps (Table 4) show two strong maxima followed by three weaker maxima. The first two positions were interpreted as iron and the following three as oxygen atoms. In spite of the different space group, the structure achieved by ADT is in fact very close to the one refined by XRPD (Haavick et al. 2000). The structure was subsequently refined by least-squares using SHELX97 (Sheldrick 2008) including partial occupancy of iron/magnesium and iron/chromium in the octahedral sites (CIF file available¹). Only soft “SADI” restraints ($\sigma = 0.05 \text{ \AA}$) were applied to Fe-O distances, independently for each Fe atom. The model obtained ab initio remains stable upon refinement with SHELXL but the refinement does not converge better than to $R1_{\text{all}} = 33.83\%$ (Table 3). Structure residuals and GooF are high when compared with X-ray diffraction, but typical for electron diffraction data (Kolb et al. 2011). In the present case dynamical effects and structure residuals are emphasized by the high density of the material and the thickness of the samples - estimated about 200-400 nm for μ -crystals and 150 nm for the FIB cuts (Kolb et al. 2011; Jacob et al. 2013). Fe^{3+} occupies a nicely

symmetrical octahedron, while Fe^{2+} is hosted inside a trigonal prismatic coordination as suggested by Dubrovinsky et al. (2003). Results and reliability of structure refinement by (ADT) electron diffraction data for an accurate determination of interatomic distances and partial occupancies have been recently reported and discussed by Birkel et al. (2010), Pignatelli et al. (2014), and Jacob et al. (2013), using either kinematical and dynamical approaches. Here, we stress that in agreement with crystallochemical expectations and with the results of Dubrovinsky et al. (2003) Fe-O distances related to Fe^{3+} are significantly shorter compared with the ones related to Fe^{2+} ($\langle 2.04 \rangle \text{ \AA}$ vs. $\langle 2.14 \rangle \text{ \AA}$). This is not the case for the structure refined by Haavick et al. (2000), where interatomic Fe^{2+} -O distances in the trigonal prismatic coordination vary significantly. Partial occupancies Fe/Cr and Fe/Mg of the Fe sites were refined up to values close to the ones estimated by WDS. While the former converged to similar values for both the refinements, the latter showed a large deviation.

Identification of the β -phase: Detailed analyses of the ADT data sets of MA-367 revealed that the β -phase is most likely isostructural with goethite FeOOH (Yang et al. 2006), which is also confirmed by a preliminary structure solution based on the ADT data. It has a primitive orthorhombic cell with parameters $a = 4.6(1) \text{ \AA}$, $b = 9.5(2) \text{ \AA}$, $c = 3.00(6) \text{ \AA}$. Extinctions are consistent with space group $Pbnm$. When α -phase and β -phase are present together they always have orientation relations with $a(\alpha) // b(\beta)$, $b(\alpha) // a(\beta)$ and $c(\alpha) // c(\beta)$ (Figs. 3c and 3d). The main feature for distinguishing the two phases is the different length of the cell parameter c .

The unknown reflections observed in the X-ray diffraction pattern of MA-367 can be explained as reflections of h-magnetite with the cell parameters determined based on our ADT analysis.

High resolution TEM confirmed that the Fe-oxide phase produced in run MA-367 is h-magnetite quenched to ambient conditions. It also confirmed the presence of a second phase, which we did not further investigate with high resolution TEM. We measured the reciprocal

lattice vectors in the TEM diffraction pattern and calculated the respective d -spacings and angles between adjacent vectors or lattice plane. The analyses were performed with selected area electron diffraction (SAED) patterns in different orientations (zone axes). The diffraction images are shown in Figure 4a and can be indexed as h-Fe₃O₄ along the $[\bar{2}1\bar{1}]$ zone axis. The basis for the indexing was the set of lattice parameters and structure obtained from the ADT analyses for h-magnetite. With the high-resolution TEM we only confirm the presence of h-magnetite we cannot prove the space group. Table 5 shows the observed d -spacings and corresponding angles between vectors for both samples. In our TEM analyses both in Mainz and at the GFZ we systematically supplemented electron diffraction with energy-dispersive X-ray spectroscopy (EDX) performed in the same locations of the foils. All the EDX measurements always yielded the same proportions of Cr, Mg, Al, and Si and there was no clear difference between the composition of the α -phase and β -phase.

In addition, we measured EEL spectra of the Fe L_{2,3}-edges of h-magnetite of run MA-367 and compare them to the spectrum of a synthetic majorite by Lenz et al. (2012) (Fig. 5). The spectrum of the iron oxide does not show the characteristic L₃ splitting that is present for majoritic garnet (Fig. 5). In addition the maxima of the L₃ and L₂ edges are shifted to lower energy compared to cubic magnetite, e.g., the maximum of the L₃ of magnetite lies at 709 eV (van Aken and Liebscher 2002). Applying the calibration by van Aken and Liebscher (2002) the averaged Fe³⁺/Fe_{total} ratio for both phases was approximately 25% (eight analyses), which is, in the case of majorite, in the range expected from other experiments (Stagno et al. 2013), but much too low for h-magnetite (Table 1). Crocombette et al. (1995), Van Aken and Liebscher (2002), and Gloter et al. (2003) observed for magnetite an unsplit broad but asymmetric L₃ peak at about 709 eV. They attribute this feature to strong charge-transfer interactions between ferrous and ferric iron (electron hopping). Thus, the calibration of Van Aken and Liebscher (2002) cannot be used to quantify the Fe³⁺ content in the oxides of our run products.

MA-376. Sample MA-376 consists of about 95% Fe-oxide phase. In this sample the Fe-oxide phase presents defect density, deformation features, and region characterized by poor crystallinity. In addition, in spite of our efforts to isolate it from atmospheric moisture, the oxide phase appears to suffer progressive weathering. We collected X-ray diffraction pattern on several opaque aggregates of MA-376 with the Rigaku diffractometer at the GFZ. The diffraction patterns (from integration of the single images) were dominated by two peaks at $2\Theta_{Cu}$ 32.7 ° and 34.3 °. However, the intensity ratios of the two peaks vary very strongly from image to image, which may indicate a strong texture effect. To get information on the whole sample we ground several aggregates and prepared them properly for the STOE transmission diffractometer. The X-ray diffractogram and the results of a LeBail refinement are shown in Figure 6. The X-ray pattern of the Fe-oxide phase in MA-376 can be explained with h-magnetite with slightly different lattice constant of $a = 9.99$, $b = 9.58$, and $c = 2.83$ Å. We did not observe reflections of goethite. This is likely due to the relative small volumetric amount of β -phase. Additionally, β -phase crystallizes in tiny nano-crystals and its cell parameters are related with cell parameters of h-magnetite. The resultant peak enlargement and overlap make β -phase signal almost completely hidden by the stronger h-magnetite signal. The final R_{Bragg} value was 1.7 %. A list of the intensity extraction (hkl) is shown in Supplemental Table 1¹. Finally we investigated the sample with ADT and HR-TEM. Both methods confirm the presence of h-magnetite but also indicate that the sample has a high defect density and cannot be used for structure determination. The diffraction image of the Fe-oxide from the foil of run MA-376 measured with HR-TEM is shown in Figure 4b and can be indexed as h-Fe₃O₄ viewed along the [001] zone axis. The ADT data sets revealed again the presence of goethite in larger amounts than in MA-367 and the same oriented intergrowth with h-magnetite.

FTIR-Spectroscopy

The total amount of hydrogen incorporated in majorite of run MA-380 has been quantified as about 500 ppm H₂O by weight by comparing the IR spectra with spectra of a synthetic majorite (Lenz et al. 2012) containing 2200 ppm H₂O by weight (Fig. 7).

Discussion

TEM analyses show that the Fe-oxide in our high-pressure run products crystallized in the structure of h-Fe₃O₄ and are quenchable to ambient conditions and stable under the experimental condition of most of the measurements (X-ray, electron beam). Microprobe analyses are consistent with about 62% of the Fe_{total} incorporated as Fe³⁺. Electron microprobe (WDS) along with analytical TEM analyses reveals that the Fe-oxide incorporated significant amounts of Cr, Mg, Al, and Si. We assigned the divalent cations to the larger Fe1 site and the three and four-valent cations to the smaller octahedral site Fe2 (Dubrovinsky et al. 2003).

This is also supported by ADT analyses. Hence we propose the following structural formula for the high-pressure Fe-oxide synthesized here: $^{\text{Fe1}}(\text{Fe}^{2+}_{0.75} \text{Mg}_{0.26})^{\text{Fe2}}(\text{Fe}^{3+}_{0.70} \text{Cr}_{0.15} \text{Al}_{0.11} \text{Si}_{0.04})_2\text{O}_4$ for MA-367 and $^{\text{Fe1}}(\text{Fe}^{2+}_{1.02})^{\text{Fe2}}(\text{Fe}^{3+}_{0.65} \text{Cr}_{0.19} \text{Al}_{0.13} \text{Si}_{0.03})_2\text{O}_4$ for MA-376.

In MA-367 the Fe-oxide forms hypidiomorphic elongated aggregates 10 – 30 μm long, mutually intergrown with majorite, the major phase of the run products. The texture of our “synthetic rock” composed of majorite, stishovite, h-Fe₃O₄, and magnesite (Fig. 1), and the uniform chemical compositions of the phases suggest that they have attained equilibrium. It is difficult to estimate the redox conditions in terms of f_{O_2} during the experiment. But at least the presence of magnesite gives us a minimum value: according to Stagno et al. (2011) at 18 GPa and T between 1500 and 1700 °C an f_{O_2} of at least 3 log units above IW is required to prevent the reduction of magnesite to diamond and MgO. Thus, we estimate that the f_{O_2} in the experimental charge was near the magnetite-wüstite buffer (that is 3-4 log units above IW). It is clear that the coexisting majorite must also incorporate Fe³⁺ to some extent; however, for simplicity, the Fe pfu for the majorite phases of this study were calculated assuming ferrous

iron only. As shown in Figure 6 for a majorite of similar composition and synthesized in the experiment MA-337 under similar conditions (Lenz et al. 2012), 25% of the total Fe can be assumed to be Fe³⁺.

The same holds true for MA-380, in which we succeeded in crystallizing large crystals by T-cycling in the first heating phases.

In MA-376 the h-magnetite is more Fe-rich than in MA-367. It has no magnesium incorporated in the Fe1 site. The oxide phase tends to decompose with time, maybe due to its Fe-richer composition. However, the transformation is not abrupt as known for the pure Fe-end-member. One and a half year after the synthesis we could still prove its presence.

Compared to MA-367, the products of run MA-376 include the end-member wadsleyite, which stores all the Mg present in the starting material. As h-magnetite in run MA-367 did incorporate Mg and did coexist with Fe, Mg – silicates we tend to interpret this observation as non-equilibrium.

The presence of small amounts of goethite was only observed in the ADT data sets neither in our X-ray diffraction data nor EMP analyses. From the oriented intergrowth with h-magnetite it is clear that there is a secondary phase, which was formed most likely during quenching.

Although we did not add pure water to the sample the powder contained adsorbed water as proven by the OH incorporation in the majorite crystals.

Implications

We report the synthesis of h-magnetite, ideally h-Fe₃O₄ with considerable amounts of substitutional cations (Cr, Mg, Al, Si) and quenchable to ambient conditions. The substitution of Fe by smaller cations may stabilize the high-pressure form during quenching. If this is true, then similar substitution mechanisms can be applied to other non-quenchable high-pressure phases to recover them for better crystal chemical and structural characterization.

Our experiments suggest that h-magnetite is a potential constituent of the Earth's mantle. It can incorporate large amounts of Cr, Mg, Al, and Si and the most of its iron is Fe³⁺. The

preservation of mantle heterogeneity as relicts of materials (most likely related to ancient subduction) that are not thermally and/or chemically equilibrated with the ambient mantle is suggested by seismic observations, and is consistent with mineral physics results, even in the deep mantle (Mosenfelder et al. 2001; Kaneshima et al. 2007; Bina 2010; Vinnik et al. 2010). Heterogeneities and anomalies observed at the transition zone level can be connected to fragments of ancient subducted lithosphere not yet thermally equilibrated where Fe-enriched, oxidized lithospheric material could be intermixed with remnants of carbonatic sediments (Nolet and Zielhuis 1994; Courtier and Revenaugh 2007). In such environments, before complete equilibration, local redox conditions may be more oxidized than that of the ambient mantle. Our syntheses performed at transition-zone pressures show that h-magnetite is stabilized in equilibrium with Fe-rich majoritic garnet at f_{O_2} close to the magnetite-wüstite buffer (i.e., 3-4 log units above IW) in a simplified system comparable to a Fe-enriched subducted lithospheric material. We observe that Cr is strongly enriched in the oxide phase with respect to the coexisting majoritic garnet with a partitioning coefficient $D_{Cr}^{Oxide/Majorite}$ of about 2.6. Our experimental results suggest that h-Fe₃O₄ can be considered as deep mantle mineral (at least in special environments). Its formation may have consequences on the chemical signature of coexisting silicates. Where h-Fe₃O₄ forms in the presence of residual carbonates, such strong fractionation could be recorded in terms of the chemical signature of silicate inclusions in deep diamonds associated with deep mantle carbonatitic melt production (Rohrbach and Schmidt 2011; Stagno et al. 2013).

This work demonstrates the advantage of electron diffraction, and particularly of the ADT method, for the structural analysis of phases that occur only as nano-sized crystals in polyphasic assemblages, even when a limited amount of material is available. ADT method also allows to recover geometrical information at the nano-scale, like the reciprocal orientation of goethite and h-Fe₃O₄ intergrowth in the Fe-oxide grains.

Acknowledgments

We thank A. Schreiber, U. Dittmann, A. Ebert, R. Schulz, and H.-P. Nabein for technical support and W. Heinrich for discussion. We also thank B. Lavina, I. Swainson, O. Tschauner, and an anonymous reviewer for their comments. ADT was supported by the Stiftung Rheinland-Pfalz für Innovation.

References cited

- Akaogi, M., Yusa, H., Shiraishi, K., and Suzuki, T. (1995) Thermodynamic properties of alpha-quartz, coesite and stishovite and equilibrium phase relations at high pressures and high temperatures. *Journal of Geophysical Research*, 100, 337 – 347.
- Belsky, A., Hellenbrandt, M., Karen, V.L. and Luksch, P. (2002) New developments in the Inorganic Crystal Structure Database (ICSD): Accessibility in support of materials research and design. *Acta Crystallographica*, B, 58, 364-369.
- Bengtson, A., Morgan, D., and Becker, U. (2013) Spin state of iron in Fe₃O₄ magnetite and h- Fe₃O₄. *Physical Review B*, 87, 155141.
- Bina, C.R. (2010) Scale limits of free-silica seismic scatterers in the lower mantle. *Physics of the Earth and Planetary Interiors*, 183, 110-114.
- Birkel, C.S., Mugnaioli, E., Gorelik, T., Kolb, U., Panthöfer, M., and Tremel, W. (2010) Solution Synthesis of a new thermoelectric Zn_{1+x}Sb Nanophase and its structure determination using automated electron diffraction tomography. *Journal of the American Chemical Society*, 132, 9881-9889.
- Bowles, J.F.W., Howie, R.A., Vaughan, D.J., and Zussman, J. (2011) In Deer, Howie, and Zussman, *Rock-forming minerals non silicates 5A*, Second edition. Geological Society of London, 927 pages, 403ff.

- Burla, M.C., Caliendo, R., Camalli, M., Carrozzini, B., Cascarano, G.L., Giacovazzo, C., Mallamo, M., Mazzone, A., Polidori, G., and Spagna, R. (2012) SIR2011: A new package for crystal structure determination and refinement. *Journal of Applied Crystallography*, 45, 357-361.
- Courtier, A.M., and Revenaugh, J. (2007) Deep upper-mantle melting beneath the Tasman and Coral Seas detected with multiple ScS reverberations. *Earth and Planetary Science Letters*, 259, 66-76.
- Crocombette, J.P., Pollak, M., Jollet, F., Thromat, N., and Gautier-Soyer, M. (1995) X-ray-absorption spectroscopy at the Fe $L_{2,3}$ threshold in iron oxides. *Physical Review B*, 52, 3143 – 3150.
- Doyle, P.A., and Turner, P.S. (1968) Relativistic Hartree-Fock X-ray and electron scattering factors. *Acta Crystallography A*, 24, 390-397.
- Dubrovinsky, L. S., Dubrovinskaia, N. A., McCammon, C., Rozenberg, G. K., Ahuja, R., Osorio-Guillen, J. M., Dmitriev, V., Weber, H. P., Le Bihan, T., and Johansson, B. (2003) The structure of the metallic high-pressure Fe_3O_4 polymorph: Experimental and theoretical study. *Journal of Physics: Condensed Matter*, 15, 7697-7706.
- Fei Y. (1996) Crystal chemistry of FeO at high pressure and temperature. In M.D. Dyar, C. McCammon, and M.W. Schaefer, Eds., *Mineral Spectroscopy: A Tribute to Roger G. Burns.*, 243-254. Geochemical Society Special Publication, St. Louis, Missouri.
- Fei, Y., and Mao, H.K. (1994) In-situ determination of the NiAs phase of FeO at high-pressure and temperature. *Science*, 266, 1678-1680.
- Fei, Y., Frost, D.J., Mao, H.K., Prewitt, C., and Häusermann, D. (1999) In situ structure determination of the high-pressure phase of Fe_3O_4 . *American Mineralogist*, 84, 203 – 206.

- Fisher, R.A., Campbell, A.J., Shofner, G.A., Lord, O.T., Dera, P., and Prakapenka, V.B. (2011) Equation of state and phase diagram of FeO. *Earth and Planetary Science Letters*, 304, 496-502.
- Gasparik, T. (1989) Transformation of enstatite – diopside – jadeite pyroxenes to garnet to garnet. *Contribution to Mineralogy and Petrology*, 102, 389 – 405.
- Gemmi, M., Fischer, J., Merlini, M., Poli, S., Fumagalli, P., Mugnaioli, E. and Kolb, U. (2011) A new hydrous Al-bearing pyroxene as a water carrier in subduction zones. *Earth and Planetary Science Letters*, 310, 422–428.
- Glazyrin, K., McCammon, C., Dubrovinsky, V., Merlini, M., Schollenbruch, K., Woodland, A., and Hanfland, M. (2012) Effect of high pressure on the crystal structure and electronic properties of magnetite below 25 GPa. *American Mineralogist*, 97, 128-133.
- Gloter, A., Douiri, A., Tencé M., and Colliex, C. (2003) Improving energy resolution of EELS spectra: An alternative to the monochromator solution. *Ultramicroscopy*, 96, 385 – 400.
- Grove, T.L. (1981) Use of FePt alloys to eliminate the iron loss problem in 1 atmosphere gas mixing experiments: Theoretical and practical considerations. *Contributions to Mineralogy and Petrology*, 78, 298 – 304.
- Haavik, C., Stølen, S., Fjellvåg, H., Hanfland, M., and Häusermann, D. (2000) Equation of state of magnetite and its high-pressure modification: Thermodynamics of the Fe-O system at high pressure. *American Mineralogist*, 85, 514 – 523.
- Hazen, R.M., and Jeanloz R. (1984) Wüstite (Fe_{1-x}O): A review of its defect structure and physical properties. *Reviews of Geophysics and Space Physics*, 22, 37-46.
- Inoue, T., Irifune, T., Higo, Y., Sanehira, T., Sueda, Y., Yamada, A., Shinmei, T., Yamazaki, D., Ando, J., Funakoshi, K., and Utsumi, W. (2006) The phase boundary between wadsleyite and ringwoodite in Mg_2SiO_4 determined by in situ X-ray diffraction. *Physics and Chemistry of Minerals*, 33, 106 – 114.

- Jacob, D., Palatinus, L., Cuvillier, P., Leroux, H., Domeneghetti, C., and Cámara, F. (2013) Ordering state in orthopyroxene as determined by precession electron diffraction. *American Mineralogist*, 98, 1526-1534.
- Kaneshima, S., Okamoto, T., and Takenaka, H. (2007) Evidence of a metastable olivine wedge inside the subducted Mariana slab. *Earth and Planetary Science Letters*, 258, 291-227.
- Kantor, Y., Kurnusov, A. , McCammon, C., and Dubrovinsky, L. (2008) Monoclinic FeO at high pressures. *Zeitschrift für Kristallographie*, 223, 461-464.
- Kolb, U., Gorelik, T., Kübel, C., Otten, M.T., and Hubert, D. (2007) Towards automated diffraction tomography: Part I—Data acquisition. *Ultramicroscopy*, 107, 507-513.
- Kolb, U., Gorelik, T., and Otten, M.T. (2008) Towards automated diffraction tomography. Part I— Cell parameter determination. *Ultramicroscopy*, 108, 763-772.
- Kolb, U., Mugnaioli, E., and Gorelik, T.E. (2011) Automated electron diffraction tomography – A new tool for nano crystal structure analysis. *Crystal Research and Technology*, 46, 542-554.
- Kondo, T., Ohtani, E., Hirao, N., Yagi, T., and Kikegawa, T. (2004) Phase transitions of (Mg,Fe)O at megabar pressures. *Physics of the Earth Planetary Interiors*, 143-144, 201-213.
- Larson, A.C. and Von Dreele, R.B. (1998) GSAS. General Structure Analysis System. Los Alamos National Laboratory. Los Alamos National Laboratory Report LAUR 86-748.
- Lavina, B., Dera, P., Kim, E., Meng, Y., Downs, R.T., Weck, P.F., Sutton, S.R., and Zhao, Y. (2011) Discovery of the recoverable high-pressure iron oxide Fe₄O₅. *Proceedings of the National Academy of Sciences*, 108, 17281 – 17285.
- Lazor, P., Shebanova, O.N., and Annersten, H. (2004) High-pressure study of stability of magnetite by thermodynamic analysis and synchrotron X-ray diffraction. *Journal of Geophysical Research*, 109, B05201.

- Lenz, S., Koch-Müller, M., Mrosko, M., Rhede, D., and Wirth, R. (2012) Crystal chemistry of synthetic majoritic garnet. Conference Abstracts, 14th International Conference Experimental Mineralogy Petrology Geochemistry - EMPG (Kiel, Germany 2012), 94.
- Morishima, H., Kato, T., Suto, M., Ohtani, E., Urakawa, S., Utsumi, W., Shimomura, O., and Kikegawa, T. (1994) The phase boundary between α - and β - Mg_2SiO_4 determined by in situ X-ray observation, *Science*, 26, 1202 – 1203.
- Mosenfelder, J.L., Marton, F.C., Ross, C.R. II, Kerschhofer, L., and Rubie, D.C. (2001) Experimental constraints on the depth of olivine metastability in subducting lithosphere. *Physics of the Earth and Planetary Interiors*, 127, 165-180.
- Mugnaioli, E., Gorelik, T., and Kolb, U. (2009) “Ab initio” structure solution from electron diffraction data obtained by a combination of Automated Diffraction Tomography and Precession Technique. *Ultramicroscopy*, 109, 758-765.
- Nolet, G., and Zielhuis, A. (1994) Low S velocities under the Tornquist-Teisseyre zone: Evidence for water injection into the transition zone by subduction. *Geophysical Research Letters*, 99, 15813-15820.
- O’Neill, H.St.C. and Palme, H. (1998) Composition of the silicate Earth: Implications for Accretion and core formation. In I. Jackson, Ed., *The Earth’s Mantle*, pp. 3-127. Cambridge University Press, U.K.
- Ono, S., Kikegawa, T. and Ohishi, Y. (2004) High-pressure phase transition of hematite, Fe_2O_3 . *Journal of Physics and Chemistry of Solids*, 65, 1527 – 1530.
- Pasternak, M. P., Nasu, S., Wada, K., and Endo, S. (1994) High-pressure phase of magnetite. *Physical Review B*, 50, 6446 – 6449.
- Pignatelli, I., Mugnaioli, E., Hybler, J., Mosser-Ruck, R., Barres, O., Kolb, U., and Michau, N. (2014) A multi-technique, micrometer- to atomic-scale description of a synthetic analog of chukanovite, $\text{Fe}_2(\text{CO}_3)(\text{OH})_2$. *European Journal of Mineralogy*, 26, 221-229.

- Rohrbach, A., and Schmidt, M. (2011) Redox freezing and melting in the Earth's deep mantle resulting from carbon-iron redox coupling. *Nature*, 472, 209-212.
- Rozenberg G. Kh., Amiel Y., Xu W. M., Pasternak M. P., Jeanloz R., Hanfland M. and Taylor R. D. (2007) Structural characterization of temperature- and pressure-induced inverse – normal spinel transformation in magnetite *Physical Review B* 75, 020102-1 - 020102-4. Doi 10.1103/PhysRevB.75.020102
- Schlitt, S., Gorelik, T.E., Stewart, A.A., Schömer, E., Raasch, T., and Kolb, U. (2012) Application of clustering techniques to electron diffraction data: Determination of unit-cell parameters. *Acta Crystallographica A*, 68, 536–546.
- Schollenbruch, K., Woodland, A.B., Frost, D.J., Wang, Y., Sanehira, T., and Langenhorst, F. (2011) In situ determination of the spinel post-spinel transition in Fe_3O_4 at high pressure and temperature by synchrotron X-ray diffraction. *American Mineralogist*, 96, 820 – 827.
- Sheldrick, G. M. (2008) A short history of *SHELX*. *Acta Crystallographica A*, 64, 112-122.
- Shu, J., Mao, H.K., Hu, J., Fei, Y., and Hemley, R.J. (1998) Single-crystal X-ray diffraction of wüstite to 30 GPa hydrostatic pressure. *Neues Jahrbuch für Mineralogie Abhandlung*, 172, 309-323.
- Stagno, V., Tange, Y., Miyajima, N., McCammon, C.A., Irifune, T., and Frost, D.J. (2011) The stability of magnesite in the transition zone and the lower mantle as function of oxygen fugacity. *Geophysical Research Letters*, 38, L19309.
- Stagno, V., Ojwang, D.O., McCammon, C.A., and Frost, D.J. (2013) The oxidation state of the mantle and the extraction of carbon from Earth's interior. *Nature*, 493, 84-90.
- Van Aken, P.A. and Liebscher, B. (2002) Quantification of ferrous/ferric ratios in minerals: New evaluation schemes of Fe L23 electron energy-loss near-edge spectra. *Physics and Chemistry of Minerals*, 29, 188 – 200.

- Vincent, R., and Midgley, P.A. (1994) Double conical beamrocking system for measurement of integrated electron diffraction intensities. *Ultramicroscopy*, 53, 271-282.
- Vinnik, L.P., Oreshin, S.I., Speziale, S., and Weber, M. (2010) Mid-mantle layering from SKS receiver functions. *Geophysical Research Letters*, 37, L24302.
- Wirth, R. (2009) Focused Ion Beam (FIB) combined with SEM and TEM: Advanced analytical tools for studies of chemical composition, microstructure and crystal structure in geomaterials on a nanometre scale. *Chemical Geology*, 261, 3-4, 217-229.
- Woodland, A.B., Frost, D.J., Trots, D.M., Klimm, K., and Mezouar, M. (2012) In situ observation of the breakdown of magnetite (Fe_3O_4) to Fe_4O_5 and hematite at high pressures and temperatures. *American Mineralogist*, 97, 1808 – 1811.
- Woodland, A.B., Schollenbruch, K., Koch, M., Boffa Ballaran, T., Angel, R. J., and Frost, D. J. (2013) Fe_4O_5 and its solid solutions in several simple systems. *Contributions to Mineralogy and Petrology*, 166, 1677 – 1686.
- Yang, H. X., Ren, L., Downs, R. T., Costin, G. (2006) Goethite, $\alpha\text{-FeO}(\text{OH})$, from single-crystal data. *Acta Crystallographica*, E62, i250-i252, <http://dx.doi.org/10.1107/S1600536806047258>.
- Zou, G., Mao, H.K., Bell, P.M., and Virgo, D. (1980) High-pressure experiments on the iron oxide wüstite (Fe_{1-x}O). *Carnegie Institute of Washington Yearbook*, 79, 374-376.

Figures

Fig. 1: Back scattered electron image of the polished run products of run MA-367 (a), run MA-380 (b), and run MA-376 (d). In the main gray-colored matrix represents majorite (Maj), the dark gray phase is stishovite (Sti), the darkest phase is magnesite (Mgs) and the light phase corresponds to the Fe-oxide. In b only majorite (gray), stishovite (dark gray) and a Fe-oxide phase (light) are present. (c) This shows a combined element mapping image, i.e., phase map of run product MA-367: in yellow the main phase majorite, red the stishovite, blue the Fe-oxide, and green the Fe-bearing magnesite; c is a slightly smaller portion of a and the black line is a guide for the eye and connects one and the same oxide grain in the two different images. (d) This is a representative BSE image of the Fe-oxide phase of run MA-376.

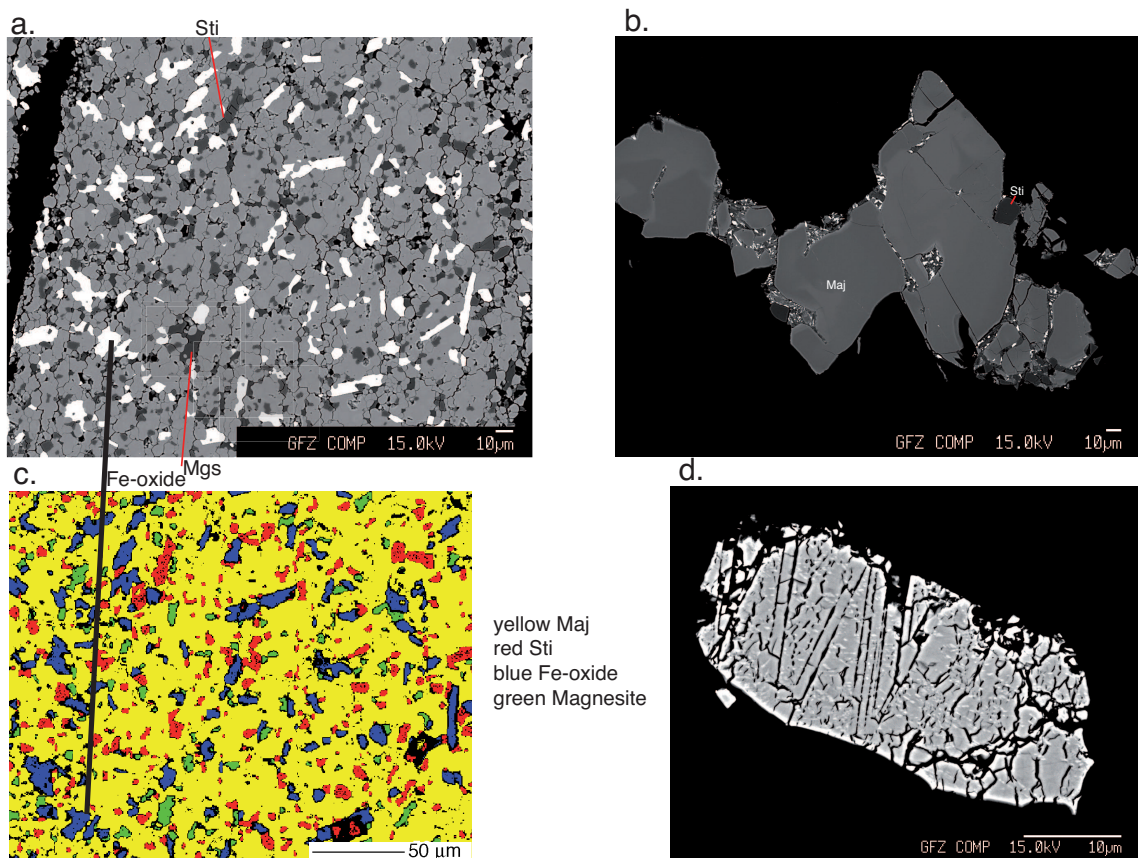


Fig.1

Fig. 2: STEM image of a part of the FIB foil cut from an Fe-oxide grain of MA-367. The foil's dimensions are $15 \times 10 \times 0.150 \mu\text{m}^3$. Two phases can be distinguished. The α -phase was identified as h-magnetite and the β -phase as goethite. The oriented intergrowth of the phases indicates that goethite is a secondary phase.

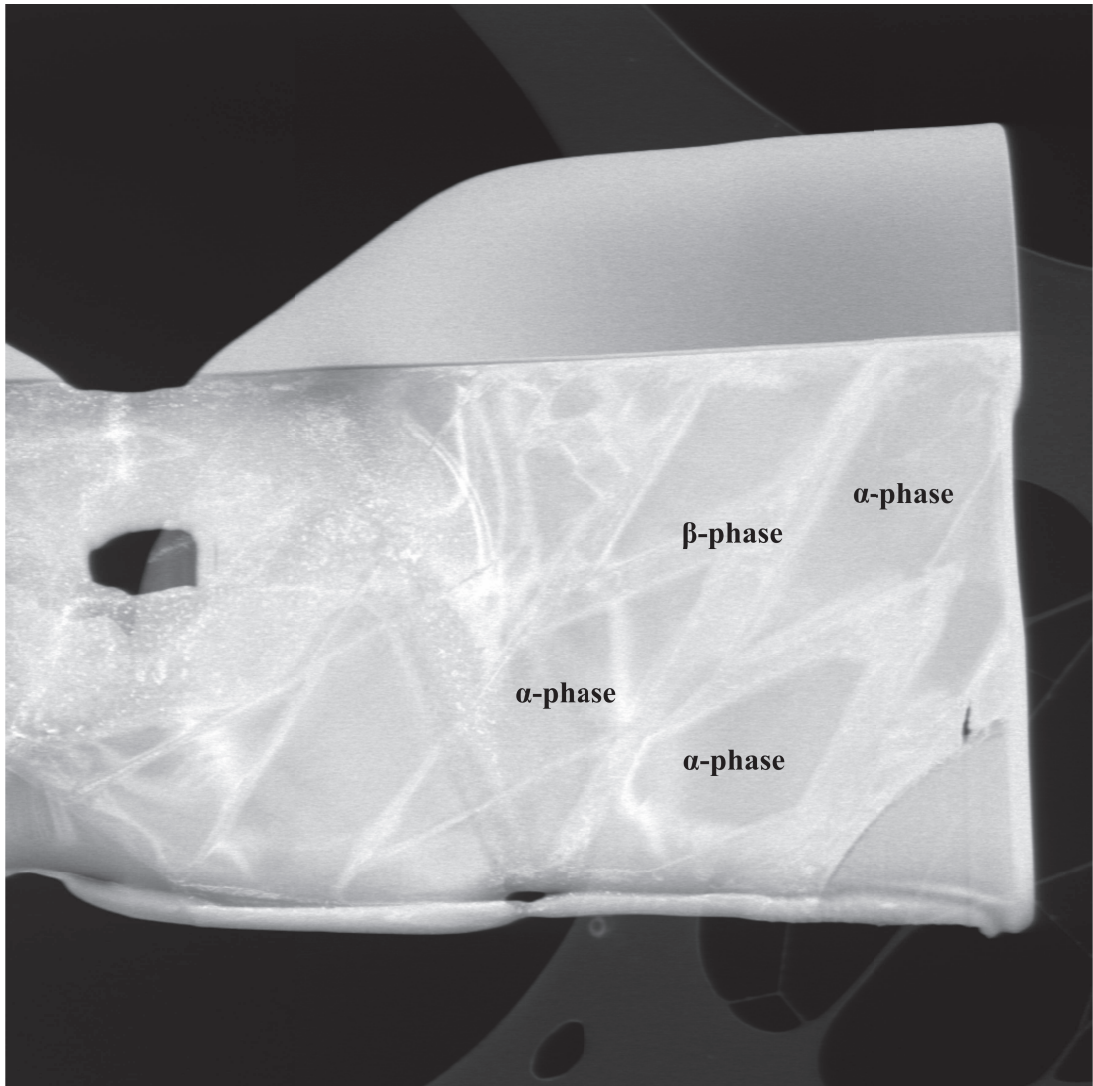


Fig. 2

Fig. 3: Three-dimensional ADT reconstructed diffraction volumes from the sample MA-367: (a-b) diffraction volume from α -phase viewed down a^* (a) and (b) down b^* ; (c-d) diffraction volume collected from an area containing both α -phase and β -phase viewed along different projections. The difference of α -phase and β -phase is evident due to the different length of c^* vector and due to the A-centered pattern of α -phase. Both phases have related crystallographic orientations. Extinctions with rule $hkl : k + l = 2n$ are recognizable for the α -phase in panels a and c. We stress that these are projections of three-dimensional diffraction volumes, and the extinctions visible in panels a and c involve full columns of reflections along $h00$.

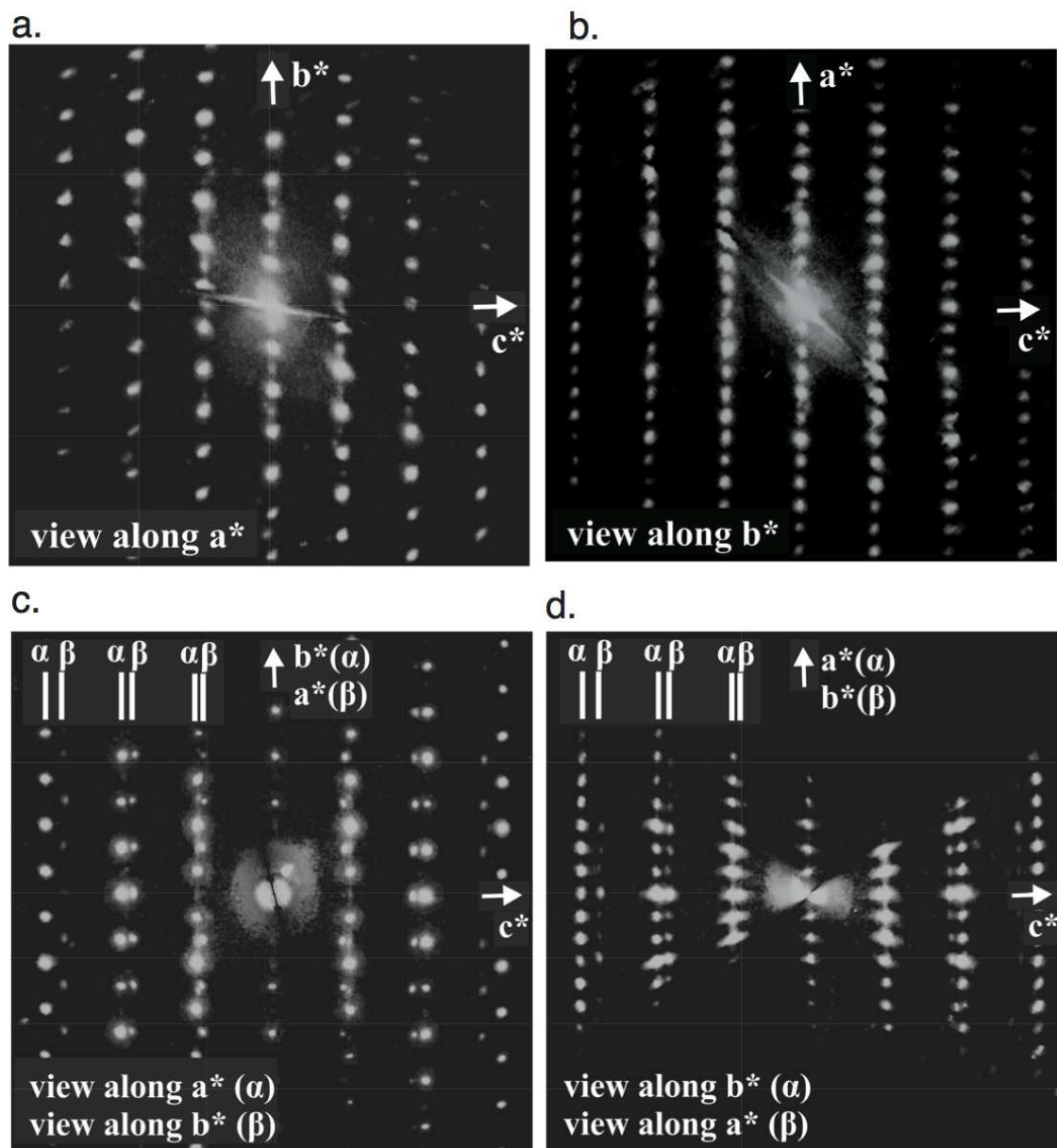


Fig. 3 a-d

Fig. 4a, b: Selected-area electron diffraction images of the mixed valence iron oxide indexed on the basis of the structure proposal obtained in this study using ADT. With this figure we prove that the iron oxide is h-magnetite.

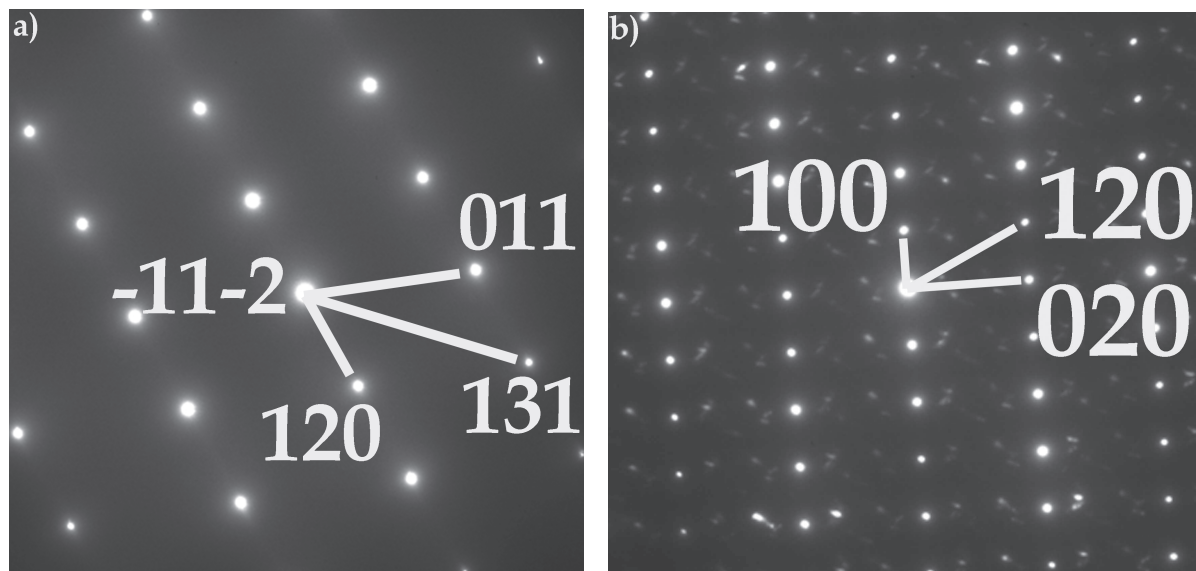


Fig.4

Fig. 5: Representative EEL spectra displaying the Fe L_{2,3}-edges of a majorite, synthesized by Lenz et al. (2012) of similar composition than in this study at 18 GPa and 1500 °C and h-Fe₃O₄ of run MA-367. The spectrum for iron oxide does not show the characteristic L₃ splitting as present for majoritic garnet. In addition the maxima of the L₃ and L₂ edges are shifted to lower energy compared to cubic magnetite, e.g., the maximum of the L₃ of magnetite lies at 709 eV (van Aken and Liebscher 2002). Applying the calibration by Van Aken and Liebscher (2002) the averaged Fe³⁺/Fe_{total} ratio was for both phases about 25% for eight analyses, which is much too low for either Fe₄O₅ or magnetite.

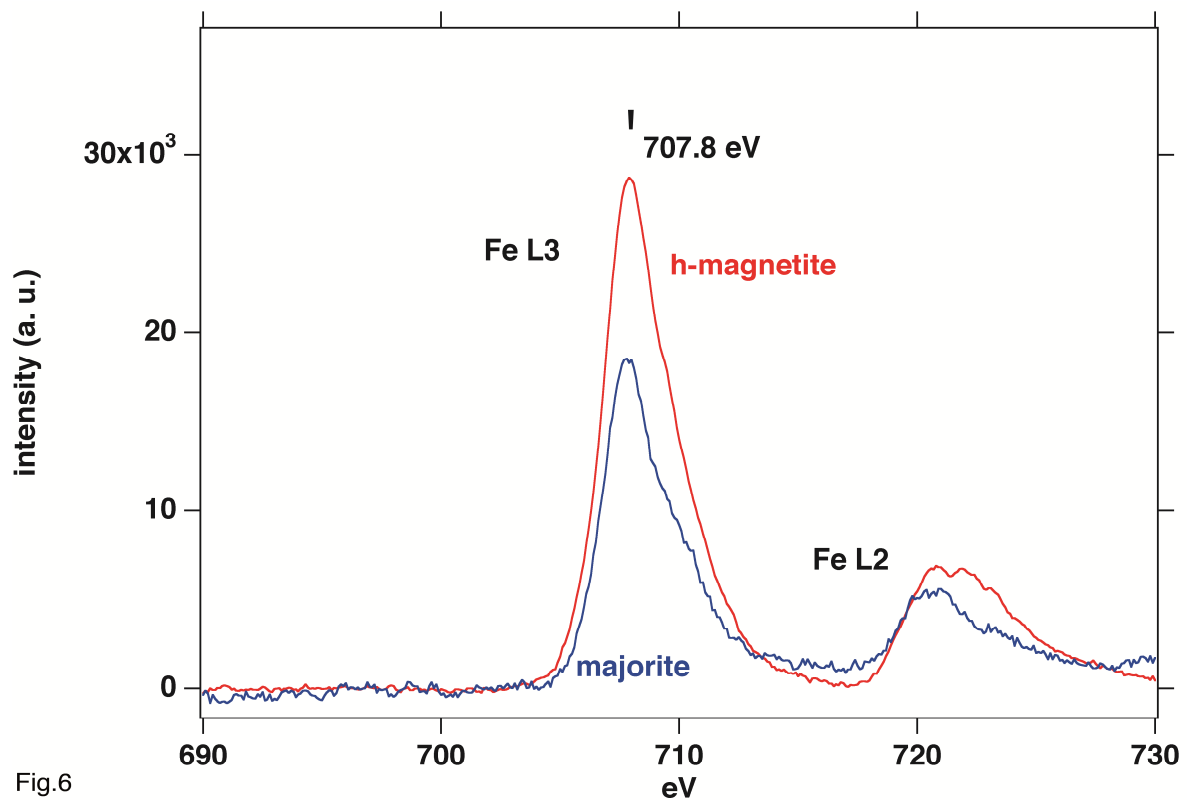


Fig. 6: Observed, calculated (LeBail Fit) and difference X-ray powder pattern of the run product MA-376 using the structural data of h-Fe₃O₄ (h-mgt) and stishovite (sti). Data were collected in transmission using a STOE STADI P diffractometer (CuK α ₁ radiation).

Convergence was achieved with R_{Bragg} in % = 1.7.

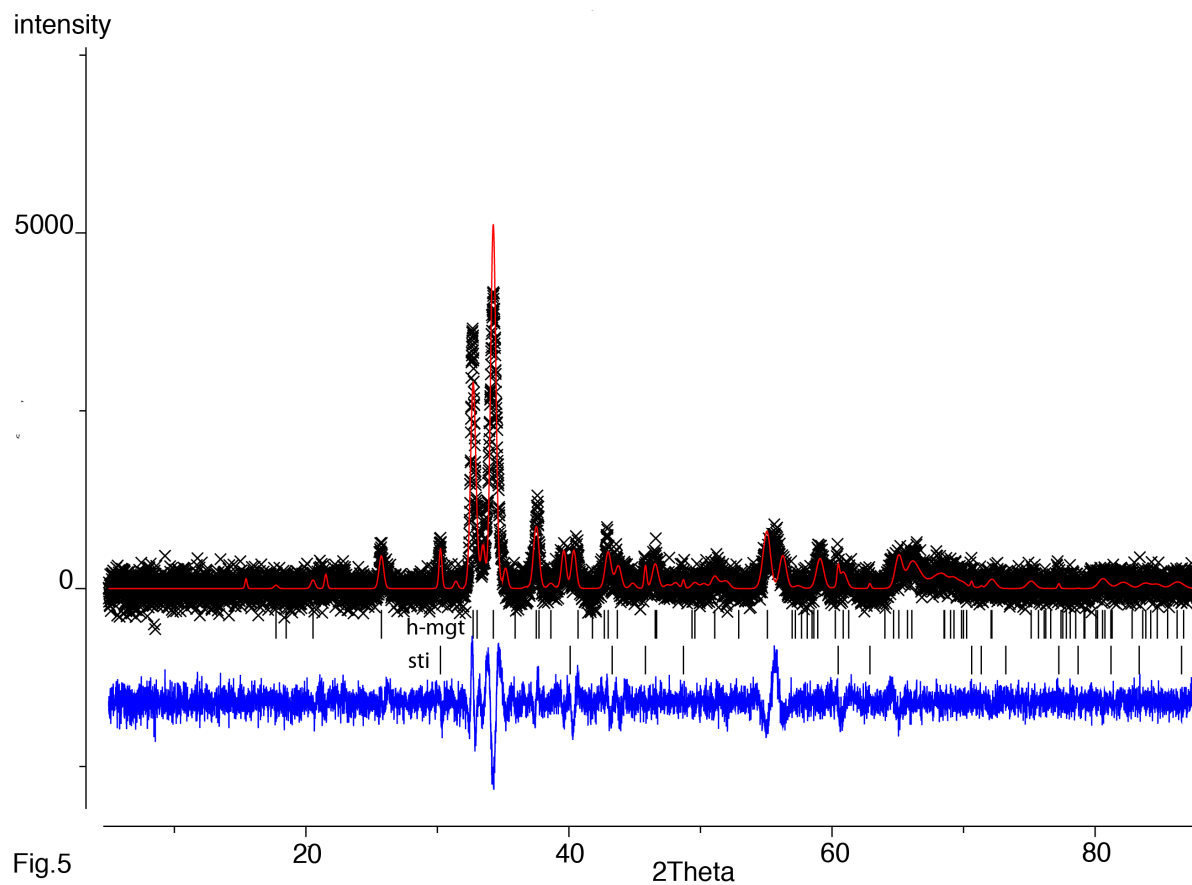


Fig.5

Fig. 7: Infrared spectra (a) of a single crystal majorite of run MA-380 showing the typical OH bands for majorite, (b) of a multi-phase aggregate of run MA-380, (c) of a single-crystal majorite, and (d) of a multi-crystal aggregate, the latter two taken from run MA-337 of Lenz et al. (2012). The starting material of this run has a similar bulk composition but water in excess (run conditions 18 GPa, 1500 °C, 3 h). All spectra show the typical OH bands around 3100 and 3600 cm^{-1} . Spectra b and d (aggregates) show in addition a broad OH band around 3400 cm^{-1} resulting from vibrations of molecular water, most probably located on the grain boundaries of the majorite aggregates. Compared to the majorite phase c of MA-337 that contained 2200 ppm H_2O by weight, majorite crystals of run MA-380 (a) contain about 500 wt ppm H_2O . In the multi-phase aggregate of MA-380 no additional absorption feature than those of OH in majorite can be observed. The thickness of the crystals was each 100 μm .

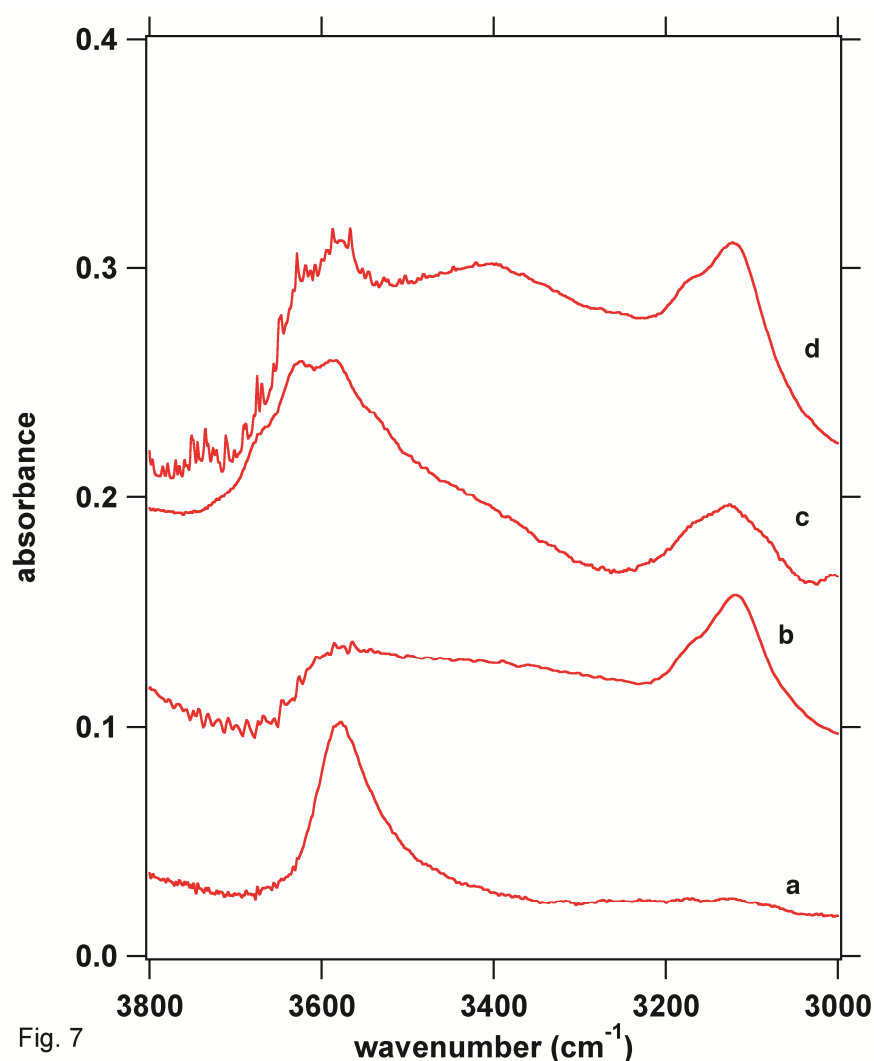
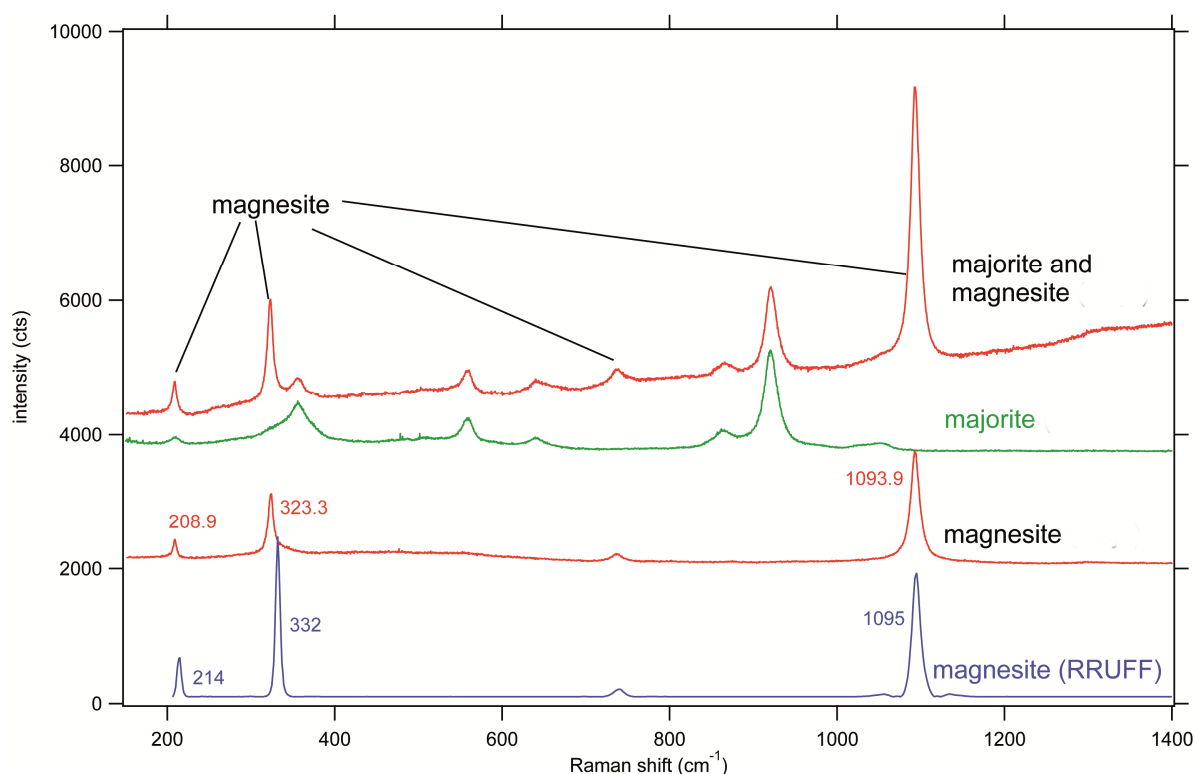


Fig. 7

Supplemental Fig.1: Raman spectra of Maj and Mgs from run MA-367 acquired on the polished section prepared for the microprobe investigations in comparison to a spectrum magnesite spectrum (X=50115) taken from the RRUFF database. They were measured with a Horiba Jobin-Yvon Labram HR 800 spectrometer (grating 1800 grooves/mm) in a backscattering configuration using a CCD detector, DPSS laser with 532 nm excitation line and an Olympus BXFM optical microscope. The spectrometer was calibrated using the Neon Plasma lines in this energy range. The numbers correspond to the peak positions. The Raman peaks of Mgs are shifted to lower wavenumbers compared to the spectrum of the endmember Magnesite of the database (RRUFF), which is in accordance to the incorporation of Fe in run MA-367. The peak position of the corresponding Raman bands of siderite are 182.1, 285, 1085.8 cm^{-1} (RRUFF ID 50349.1).



Tables

Table 1: Electron microprobe analyses and calculated cations pfu (n= number of measurements; numbers in parenthesis are 1σ standard deviation on the last digits)

MA-367	h-Fe ₃ O ₄ n = 13	majorite n = 20	stishovite n = 4	carbonate* n=3
FeO	72.07(14)	17.33(24)	0.70(16)	15.99
Cr ₂ O ₃	10.21(4)	1.98(14)	0.15(6)	-
MgO	4.93(9)	19.86(19)	0.24(9)	36.10
Al ₂ O ₃	4.89(5)	18.95(5)	1.81(8)	-
SiO ₂	2.31(7)	43.11(17)	1.35(9)	-
Σ	94.41	101.26	100.54	52.09
	4 O atoms	12 O atoms	2 O atoms	3 O atoms
Fe ²⁺	0.75(1)	1.05(4)	0.01(1)	0.20
Fe ³⁺	1.39(1)	-	0.00(1)	-
Cr ³⁺	0.29(1)	0.11(3)	0.00(1)	-
Mg	0.26(1)	2.14(2)	0.00(1)	0.80
Al	0.21(1)	1.61(1)	0.02(1)	-
Si	0.08(1)	3.11(2)	0.98(1)	-
Σ	3.00	8.02	1.01	1

MA-376	h-Fe ₃ O ₄ n = 12	wadsleyite n = 3
FeO	73.01(16)	0.19(7)
Cr ₂ O ₃	12.16(6)	0.02(1)
MgO	0.02(9)	54.82(16)
Al ₂ O ₃	5.45(8)	0.09(1)
SiO ₂	1.35(9)	41.88(14)
Σ	91.99	97.00
	4 O atoms	4 O atoms
Fe ²⁺	1.02(1)	0.01(1)
Fe ³⁺	1.30(1)	-
Cr ³⁺	0.37(1)	0.00(1)
Mg	0.00(1)	1.97(2)
Al	0.25(1)	0.01(1)
Si	0.05(1)	1.01(1)
Σ	3.00	3.00

* carbon was calculated by stoichiometry

Table 2: Extinction rules for space groups *Bbmm* and *Amam* (the “=2n” is omitted)

Point group (<i>mmm</i>)	<i>hkl</i>	<i>OkI</i>	<i>h0I</i>	<i>hk0</i>	<i>h00</i>	<i>Ok0</i>	<i>00I</i>
<i>mm</i>	<i>h + l</i>	<i>k, l</i>	<i>h + l</i>	<i>h</i>	<i>h</i>	<i>k</i>	<i>l</i>
<i>Amam</i>	<i>k + l</i>	<i>k + l</i>	<i>h, l</i>	<i>k</i>	<i>h</i>	<i>k</i>	<i>l</i>

Table 3: Experimental details about ADT data sets and related ab initio structure solutions and refinements.

	Crystal 1	Crystal 2
a (Å)		9.8(2)
b (Å)		9.6(2)
c (Å)		2.87(6)
α (°)		90
β (°)		90
γ (°)		90
Space group		<i>Amam</i>
Wavelength of radiation (Å)	0.0197	0.0197
Max resolution (Å)	0.80	0.80
Unique reflections	121	171
Reflection completeness (%)	69	97
R_{int} (%)	17.77	20.32
Range of h, k, l	$-10 < h < 10$	$-12 < h < 12$
	$-12 < k < 12$	$-12 < k < 12$
	$-3 < l < 3$	$-3 < l < 3$
$R_{(\text{SIR2011})}$	24.26	24.36
$R1_{(4\sigma)}$ (%)	33.11	38.33
$R1_{\text{all}}$ (%)	33.83	39.77
GooF	5.248	4.500
Least-squares parameters	16	16

Table 4: Ab initio solution by direct methods (SIR2011) and structure refined by least squares (SHELX97) on the basis of ADT electron diffraction data.

Ab initio solution – SIR2011						Refinement – SHELX97				
Atom	Height	Multipl.	x	y	z	x	y	z	Fe : Cr	U(iso)
name	(e/Å ³)								Fe : Mg	(Å ²)
Fe1	3.59	8	0.423	0.630	1	0.431	0.633	1	3.3 : 1	0.005
Fe2	3.54	4	¼	0.388	½	¼	0.376	½	1.5 : 1	0.012
O1	1.70	4	½	½	½	½	½	½		0.032
O2	1.60	4	¼	0.537	1	¼	0.540	1		0.104
O3	1.46	8	0.393	0.266	1	0.378	0.275	1		0.022
1 st ghost	0.67									

Notes: First column: atom name; second column: value of the maxima recognized in the potential map (the 1st ghost height is reported for comparison); fourth to sixth columns: fractional coordinates of the solution proposed ab initio; seventh to ninth columns: fractional coordinates refined by least squares; tenth column: partial occupancy Fe:Cr and Fe:Mg; eleventh column: isotropic thermal factor U. Solution and refinement from “Crystal 1” data.

Table 5: Transmission electron microscopic analyses; numbers in parentheses behind the experimental data are 1σ standard deviation on the last digits

MA-367			
exp	h-Fe ₃ O ₄	exp	h-Fe ₃ O ₄
4.220(9)	4.294 (120)	47.08(5)°	47.0° (131)/(120)
2.716(9)	2.749 (011)	27.95(5)°	28.5° (131)/(011)
2.053(9)	2.084 (131)		
MA-376			
exp	h-Fe ₃ O ₄	exp	h-Fe ₃ O ₄
9.948(6)	9.990 (100)	26.05(6)°	25.62° (1209)/(010)
4.738(6)	4.790 (020)	63.95(6)°	64.38° (120)/(100)
4.291(6)	4.319 (120)		

Notes: The calculated *d*-spacings of h-Fe₃O₄ are based on the structural proposal and the lattice parameter (Å) derived in this study: *a* 9.8 *b* 9.6 *c* 2.87 for MA-367 and *a* 9.9 *b* 9.58 *c* 2.83 for MA-376.